PSEUDO-DUCTILITY IN 0-DEGREE FIBRE DOMINATED CFRP THROUGH PLY WEAKENING

J. Sun[1.a], M. F. Pernice[1.b], O. Bacarreza[1.c] and P. Robinson[1.d]

[1]Department of Aeronautics, Imperial College London, SW7 2AZ, London, UK
[a]jingjing.sun13@imperial.ac.uk, [b]m.pernice@imperial.ac.uk, [c]o.bacarreza-nogales@imperial.ac.uk, [d]p.robinson@imperial.ac.uk

Keywords: pseudo-ductility, ply modification, unidirectional composite, multi-directional composite

Abstract

Previous research has demonstrated pseudo-ductile tensile response can be achieved by introducing periodic across-width ply cuts, perpendicular to selected 0° plies, in both unidirectional (UD) and quasi-isotropic (QI) laminates. The inserted discontinuities initiate progressive delamination at the interface between the cut and pristine (uncut) plies. The tensile stress-strain curve consists of an initial almost linear stage with high modulus, a flat plateau stage and a final strain-hardening stage. This paper presents the enhanced pseudo-ductile performance achieved by introducing dispersed periodic short perforations in the UD laminates. Perforations with precisely controlled length were cut into the constituent prepregs using a laser milling machine. UD laminates containing perforations in selected plies exhibit high initial modulus, a softening stage prior to a final strain-hardening stage, all connected by smooth transitions. The dominant failure mechanism in this case was debonding surrounding the discontinuous perforated fibre bundles. This failure mechanism was successfully transferred to 0° fibre-dominated multi-directional (MD) laminates with perforations introduced in the middle 0° plies, and thereby provided pseudo-ductile performance.

1. Introduction

Using large safety factors when designing with conventional brittle CFRP composites undermines the advantages derived from their superior mechanical properties, such as high specific stiffness and strength, and their outstanding resistance to corrosion and fatigue. A number of innovative CFRP laminate architectures have demonstrated the potential to achieve pseudo-ductility by provoking damage mechanisms, such as interlaminar matrix shearing, fibre straightening, fibre pull-out and fibre rotation, through suitable tailoring of the composite architecture [1-4]. Most of these strategies to achieve pseudo-ductility were successfully implemented in unidirectional (UD) laminates but have not been investigated for multi-directional (MD) laminates, which offer a wider scope of application in practical engineering structures.

The authors have previously shown that a UD CFRP laminate, made of a single carbon fibre system, can display a pseudo-ductile response when periodic continuous ply cuts, transverse to the 0° fibres, are introduced into the middle plies of the layup [5]. This cut-ply approach was also shown to be feasible to induce pseudo-ductility in QI laminates [6]. In this case, the 4-ply UD cut-ply laminate investigated in [5] was used as a sublaminate in the 90°, 0°, +45° and -45° directions to form a QI laminate.

This paper investigates the potential to improve the pseudo-ductility in UD laminates using a laser perforation method. Periodic perforations were designed using the analytical model proposed in [5] and were introduced in UD laminates and in 0° fibre-dominated MD laminates, to evaluate the

feasibility of transferring the failure mechanism from UD to MD perforated laminates. The failure mechanism was investigated using interrupted tests accompanied with ultrasonic C-scan and X-ray scan inspection.

2. Experimental

2.1. Material

The material used was Hexply® M21/35%/198/T800s carbon fibre/epoxy prepreg with nominal cured ply thickness of 0.184 mm. The mechanical properties are summarised in Table 1.

Table 1. Mechanical properties of UD M21/T800s prepreg.

Fibre volume fraction Vf (%)	Elastic modulus E_0 (GPa)	Strain to failure ε (%)	Tensile Strength σ_0 (MPa)	Matrix interfacial shear strength τ_y (MPa)	Mode II fracture toughness G_{IIC} (kJ/m^2)
56.9	160	2.0	2900	97	1.7

2.2. Specimen details

The UD and 0° fibre-dominated MD laminates were manufactured and bonded with glass/epoxy (GFRP) cross-ply end tabs, based on the ASTM D3039 standard [7]. The stacking sequences of the perforated UD and MD laminates are $[0°/0°_p/0°_p/0°]$ and $[90°/+45°/-45°/0°/0°_p]_s$ (the subscript 'p' denotes ply with perforations), respectively. The latter can be regarded as sandwiching two 0° perforated plies into QI laminates, so that the pristine 0° plies of the QI blocks separate the perforated 0° plies from the outer off-axis plies and create a $0°/0°_p$ interface in the MD specimen, similar to that of the UD perforated laminates.

In [5], ply cuts were introduced transverse to the 0° ply, across the entire width of the specimen. In this work, the cuts were discontinuous across the specimen width. Lines of perforations were repeated periodically along the fibre direction, as done previously for continuous cut plies [5]. The perforation pattern was selected using the analytical model proposed in [5] while assuming interlaminar and translaminar fracture, occurs at the four surfaces around the perforated fibre bundles. The pseudo-yielding stress, σ_y, is related to the mode II interlaminar fracture toughness, G_{IIC}, and is calculated from Eq. (1), based on fracture mechanics.

$$\sigma_y = \sqrt{\frac{2wG_{IIC}A_f E_0 E_f}{{A_0}^2 E_0 - A_0 A_f E_f}} \quad (1)$$

where E_0 and E_f are the effective longitudinal elastic moduli before and after the fibre bundle circumferential debonding, A_0 and A_f are the cross-sectional area of the entire laminate and the unperforated region, w is the overall perimeter of the debonded bundles.

A perforation length of 5 mm was selected. Schematics of the perforation pattern in the 0° plies of the UD and MD specimens are shown in Fig. 1. The distances between adjacent perforations in the longitudinal and transverse directions are 10 mm and 5 mm respectively, in both UD and MD specimens. Compared with the cut ply specimens which contain no continuous fibres in the cut plies [5], this perforation pattern provides 50% (in volume) of continuous fibres in the perforated 0° plies. Perforations with precisely controlled length were produced in the prepreg using a laser milling technique. Perforations in the two middle perforated plies were aligned in both UD and MD cases. The dimensions of the UD and MD specimens are 250 mm/20 mm/0.74 mm and 200 mm/30 mm/1.84 mm in length/width/thickness, respectively. Noting that the UD specimens were 5 mm wider than the standardized ones [7], to encompass two perforations in the transverse direction.

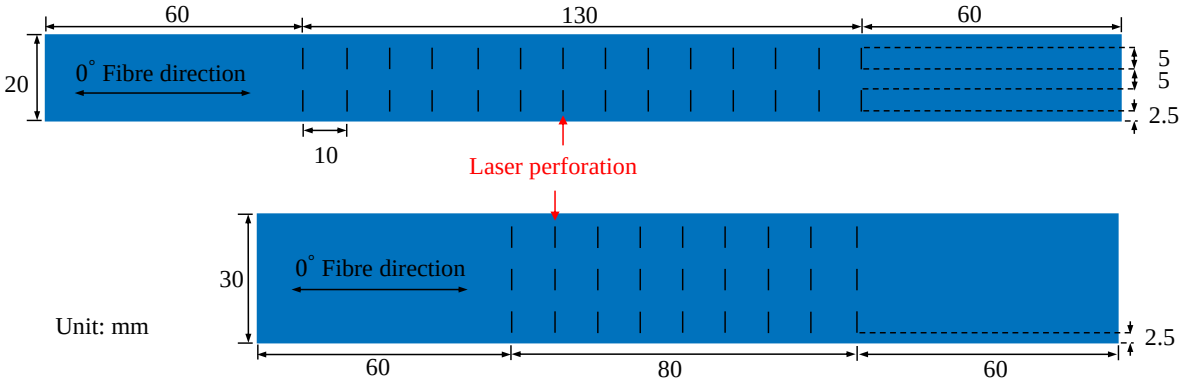

Figure 1. Schematic top views of the perforated plies in the UD (top) and the **0°** fibre-dominated MD (bottom) specimens.

2.3. Experimental procedure

Static tensile tests were performed in a 250 kN Instron machine equipped with hydraulic wedge type grips. The uniaxial tensile loading was applied at a crosshead displacement speed of 2 mm/min. At least five specimens were tested for each configuration. Four specimens were tested to ultimate failure. Strains were measured by an Imetrum optical strain gauge system and a GOM Digital Image Correlation (DIC) system. A Mistras Acoustic Emission (AE) system accompanied with a broadband (WD) acoustic transducer, was used to capture the acoustic events initiated from damage and record the associated acoustic energy in one MD specimen test. The placement of the optical strain gauge target points, DIC speckle pattern and the AE transducer (in the MD case) is schematically shown in Fig. 2. The damage modes in the MD configuration were analysed by performing ultrasonic C-scan and X-ray scan inspections of a specimen tested up to a load level close to the ultimate fracture.

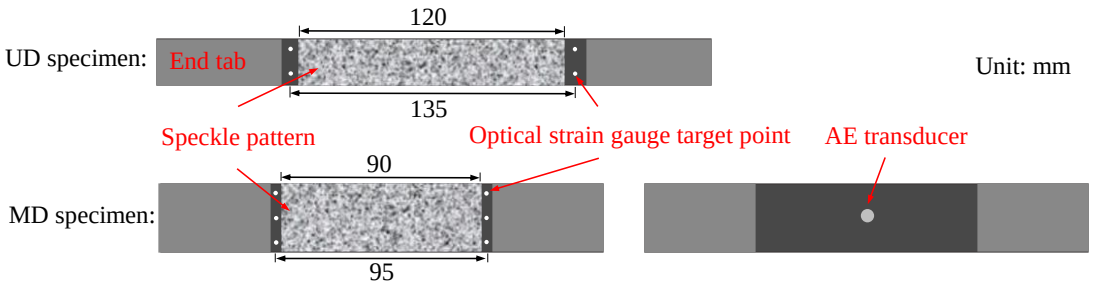

Figure 2. Schematics of the placement of the DIC speckle pattern, Imetrum optical strain gauge target points and AE transducer on UD (top) and MD specimens (bottom).

3. Results and Discussion

The tensile stress-strain curve for a UD perforated specimen and the corresponding strain maps captured from the DIC system at selected stress levels are shown in Fig. 3. Four analytical reference lines are plotted to assist the analysis. The reference lines represent: the modulus of an intact UD specimen, E_0 (in yellow); the modulus of a UD specimen with perforated fibre bundles completely delaminated from the residual material, 75% E_0 (in purple); the tensile strength of the remaining material after the complete debonding, 0.75% σ_0 (in green); and the pseudo-yield stress associated with the onset of circumferential perforated fibre bundle debonding, σ_y (in red).

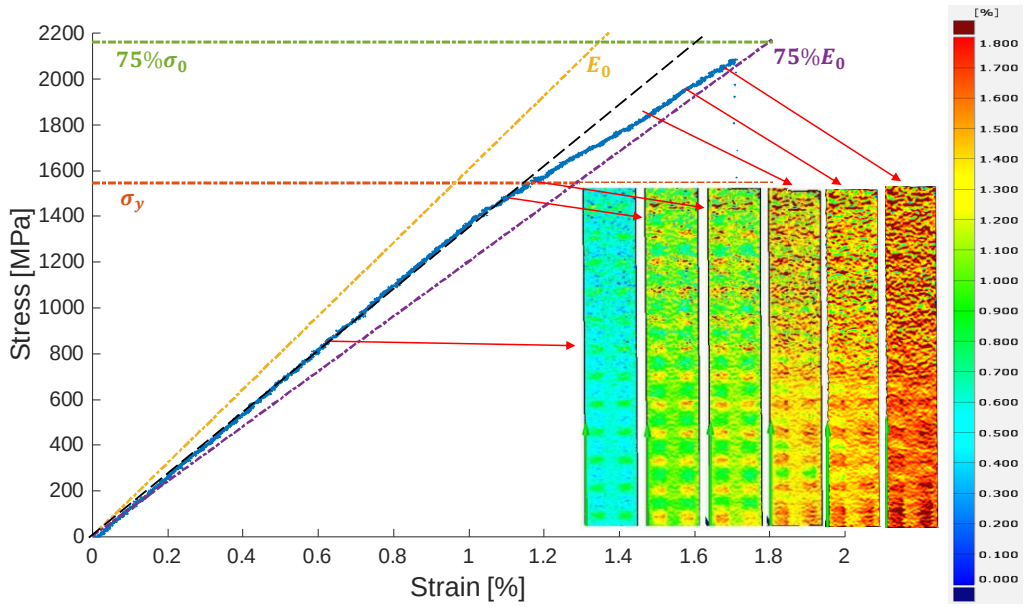

Figure 3. Tensile stress-strain curve of a 4-ply UD perforated specimen and DIC strain maps at different stress levels. The black dash line indicates the initial modulus of the initial stage.

The good agreement between the experimental and analytical pseudo-yield stress indicates that the initiation of debonding occurs on the perimeter around the perforated bundles as assumed in the analytical model. However the stress-strain curve does not exhibit a plateau following the initial 'yielding'. This is likely to be due to: (1) variation in toughness associated with the progression of debonding of the individual fibre bundles initiated by the perforations and (2) a rising toughness as the bundles debonded length increases partially on the sides of the bundles where translaminar fracture occurs and is likely to encounter significant fibre bridging. The DIC strain maps indicate the debonded

area (shown in red and yellow in Fig. 3) is expanding even at stress levels close to the ultimate fracture point.

A pseudo-ductile tensile stress-strain curve with a short softening stage was achieved in the MD perforated specimen as shown in Fig. 4(a). The good correlation between the analytical and experimental pseudo-yield stress, σ_y, indicates the failure mechanisms of debonding around the perforated fibre bundles observed in the UD configuration was successfully transferred to the MD specimen. The normalized acoustic energy accompanied with the damage events during the loading process is shown in Fig. 4 (b). Dense acoustic events with less than 20% normalized AE energy were identified and the amount of the low energy acoustic events reduces after the onset of debonding (i.e. the pseudo-yielding point). These events are primarily arisen from the cracks at the resin-filled perforated locations and cracks in the 45° plies as shown in the X-ray scanning diagram of a specimen loaded to a stress level close to the ultimate fracture (see Fig. 5). In addition, the fibre directional cracks with varying lengths located at the boundaries between the perforated and pristine fibre bundles indicate debonding initiated from the dispersed perforations propagate non-uniformly along the fibres. The ultrasonic C-scan diagram from an interrupted test shown in Fig. 6 indicates the zones of interlaminar delamination initiated from the perforations (shown as black lines).

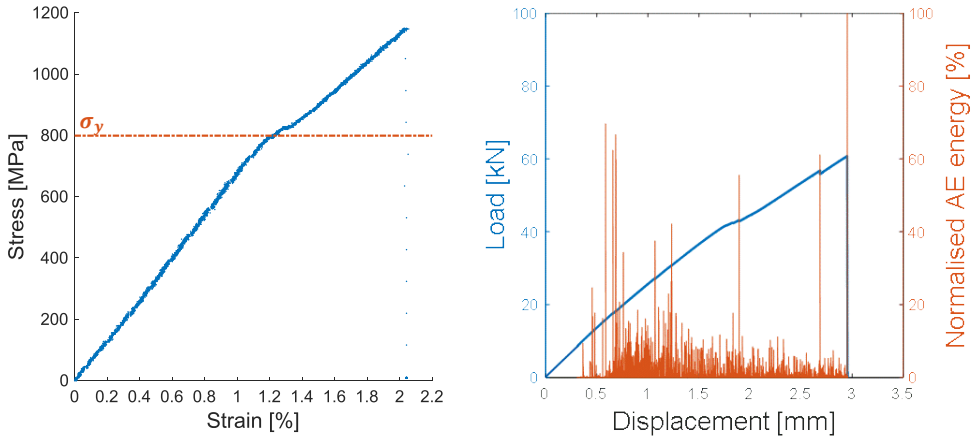

Figure 4. (a) Tensile stress-strain curve and (b) load-displacement curve with in-situ normalized acoustic energy of damage events in a MD perforated specimen.

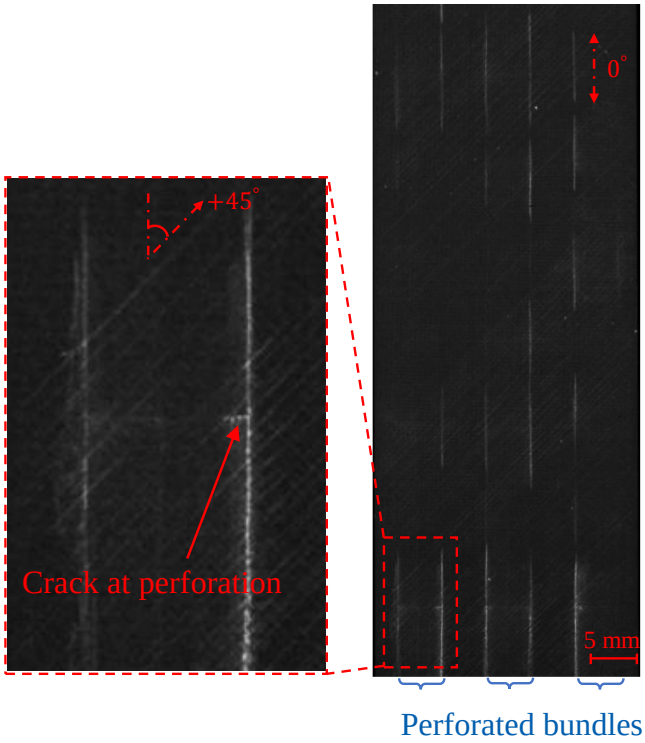

Figure 5. X-ray scanning diagram indicating cracks in the 45° plies and the resin-filled perforation location and longitudinal cracks at the boundaries of adjacent 5 mm fibre bundles in an interruptedly tested MD specimen.

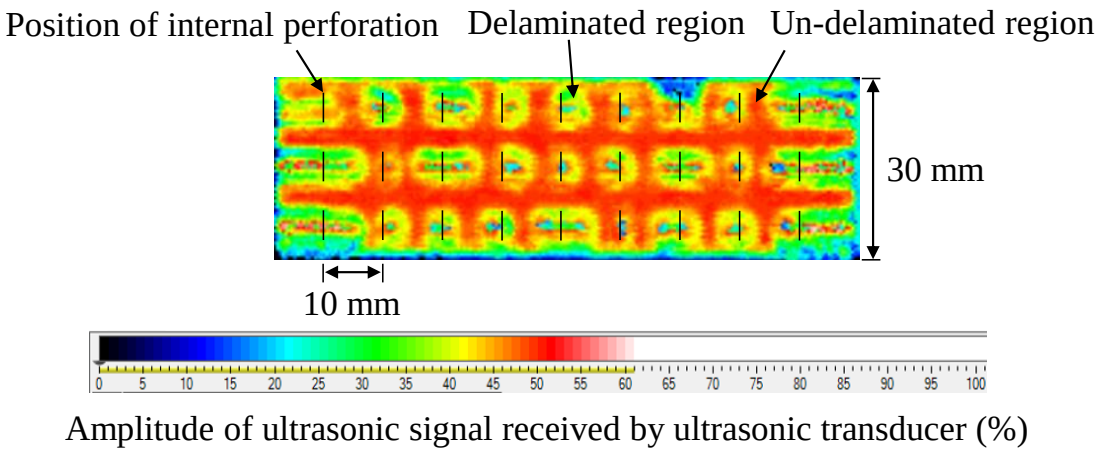

Figure 6. Ultrasonic C-scan diagram of a MD specimen tested to a stress level close to the ultimate failure showing the amplitude of signal transferred back to the ultrasonic transducer. The black lines indicate the position of the internal perforations.

4. Conclusions

Perforations were introduced in the central plies in a UD and a 0° fibre-dominated MD laminates. The ply perforations were introduced in order to achieve a pseudo-ductile response under tension. Testing showed that both UD and MD specimens exhibited pseudo-ductile performance using the perforation strategy. The dominant failure mechanism was debonding involving interlaminar and translaminar

fracture. Debonding was initiated from the introduced perforations once the tensile load reached a critical level and propagated along the 0° fibre direction at the interface between the perforated bundles and the surrounding continuous material.

Acknowledgments

This work was funded under the UK Engineering and Physical Sciences Research Council Programme Grant EP/I02946X/1 on High Performance Ductile Composite Technology in collaboration with the University of Bristol. Supporting data can be requested from the corresponding author, but may be subject to confidentiality obligations.

References

[1] T.P. Niebel, D. Carnelli, M.R. Binelli, et al. Hierarchically roughened microplatelets enhance the strength and ductility of nacre-inspired composites. Journal of the mechanical behavior of biomedical materials, 60:267-277, 2016.

[2] S. Pimenta, P. Robinson, Wavy-ply sandwich with composite skins and crushable core for ductility and energy absorption. Composite structures, 116: 364-376, 2014.

[3] G. Czél, M.R. Wisnom. Demonstration of pseudo-ductility in unidirectional hybrid composites made of discontinuous carbon/epoxy and continuous glass/epoxy plies. Composites Part A, 72:75-84, 2015.

[4] J. Fuller, Wisnom M.R., Pseudo-ductility and damage suppression in thin ply CFRP angle-ply laminates, In: Proceedings of ICCM 19 Conference. Montreal, July, 2013.

[5] J. Sun, O. Bacarreza and P. Robinson. Pseudo-ductility in UD CFRP through interlaminar and ply weakening. ECCM 17, Munich, 26-30 June 2016.

[6] J. Sun, O. Bacarreza and P. Robinson. Pseudo-ductility in quasi-isotropic CFRP through ply weakening. ICCM 21, Xi'an, 20-25 August 2017.

[7] ASTM D3039/D3039M-17 Standard Test Method for Tensile Properties of Polymer Matrix Composite Materials, West Conshohocken, PA, 2017.